GEOPHYSICS, VOL. 75, NO. 6 (NOVEMBER-DECEMBER 2010); P. E227–E234, 10 FIGS., 1 TABLE.
10.1190/1.3508874

Dynamic elastic properties of coal

Anyela Morcote[1], Gary Mavko[2], and Manika Prasad[3]

ABSTRACT

Laboratory ultrasonic velocity measurements of different types of coal demonstrate that their dynamic elastic properties depend on coal rank and applied effective pressure. In spite of the growing interest in coal beds as targets for methane production, the high abundance in sedimentary sequences and the strong influence that they have on seismic response, little data are available on the acoustic properties of coal. Velocities were measured in core plugs parallel and perpendicular to lamination surfaces as a function of confining pressure up to 40 MPa in loading and unloading cycles. P- and S-wave velocities and dry bulk and dry shear moduli increase as coal rank increases. Thus, bituminous coal and cannel show lower velocities and moduli than higher ranked coals such as semianthracite and anthracite. The V_P-V_S relationship for dry samples is linear and covers a relatively wide range of effective pressures and coal ranks. However, there is a pressure dependence on the elastic properties of coal for confining pressures below 5 MPa. This pressure sensitivity is related to the presence of microcracks. Finally, the data show that coal has an intrinsic anisotropy at confining pressures above 5 MPa, the closing pressure for most of the microcracks. This intrinsic anisotropy at high pressures might be due to fine lamination and preferred orientation of the macerals.

INTRODUCTION

Coal is a carbonaceous rock formed by compaction and diagenesis of vegetation remains. It is classified into humic and sapropelic varieties. Humic coal is derived primarily from woody tissue whereas sapropelic coal is derived primarily from spores, pollen, and algae and is subdivided into cannel and boghead coal.

Coalification is the process by which plant material is transformed into coal. This process involves an increase in temperature and pressure, causing chemical and physical changes in coal structure. The degree of maturation during this process determines the coal rank. From lowest to highest, ranks in humic coals are lignite, sub-bituminous coal, bituminous coal, semianthracite, and anthracite. Carbon-based minerals in low-ranked coals (lignite and sub-bituminous coals) show large porosity, are randomly oriented, and present relative strong crosslinks. In contrast, bituminous coal shows lower porosity and minerals are oriented parallel to one another and present weak crosslinks. Anthracite coal, on the other hand, presents a strong orientation of the minerals and strong crosslinks between minerals (Van Krevelen, 1993). At the macroscopic level, coal presents bright bands and dull bands, which have different texture, composition, and physical properties. In general, bright bands are shiny and brittle whereas dull bands are soft and friable.

During the coalification process, large volumes of methane are generated and stored within the coal. Methane stored in coal beds has been exploited at commercial rates and represents an active play with a great potential for future development. However, there is still little data available on the acoustic properties of coal. Prior work in this regard includes laboratory studies of bituminous coal. Greenhalgh and Emerson (1986) measure compressional- and shear-wave velocities at atmospheric conditions on 143 core samples oriented parallel and perpendicular to lamination surfaces. Yu et al. (1991, 1993) report measurements of acoustic velocities in dry and water-saturated specimens as confining pressure increased from 2 to 40 MPa. Castagna et al. (1993) report compressional- and shear-wave velocities for two bituminous coal samples from Utah as confining pressure increased from 3.4 to 103 MPa. Yao and Han (2008) measure ultrasonic velocities in four coal samples and three silty coal samples.

This paper presents for the first time dynamic elastic properties of coals with different thermal maturity degrees, or ranks, as a function of increasing confining stress. Velocities of dry coal samples of different ranks were measured as confining pressure increased from 0 to 40 MPa. We studied a total of nine core plugs: two of cannel

Manuscript received by the Editor 31 January 2010; revised manuscript received 22 June 2010; published online 8 December 2010.
[1]Formerly at Stanford University, Stanford, California, U.S.A.; presently at OHM-Rock Solid Images, Houston, Texas, U.S.A. E-mail: a.morcote@ohmrsi.com.
[2]Stanford University, Department of Geophysics, Stanford Rock Physics Laboratory, Stanford, California, U.S.A. E-mail: mavko@stanford.edu.
[3]Colorado School of Mines, Center for Rock Abuse, Department of Petroleum, Engineering, Golden, Colorado, U.S.A. E-mail: mprasad@mines.edu.

coal, three of bituminous coal, two of semianthracite, one of anthracite, and one powder sample from bituminous coal.

EXPERIMENTAL TECHNIQUE

Cylindrical core plugs, 2.5 cm in diameter and 2.0–4.0 cm in length, were taken in two directions: parallel (90°) and perpendicular (0°) to lamination surfaces. The powder from bituminous coal was precompressed at 0.6 MPa. Nine core plugs were dried for 48 hours in an oven at 60 °C.

Porosity was measured using a helium porosimeter. This instrument measures porosity by displacement of pore volume by helium at known pressures. Grain and pore volumes were determined by Boyle's Law. In this method, the grain volume is calculated from the volume of helium and the total volume is obtained from the dimensions of the plugs.

The P-wave (V_P) and S-wave (V_S) velocity measurements were taken using the pulse transmission technique (Birch, 1960). Velocities were measured parallel and perpendicular to bedding planes with the propagation and vibration directions aligned parallel and normal to lamination. In samples with no visible lamination (powder and anthracite), velocities were measured in only one arbitrary direction.

The experimental setup consists of a digital Tektronix (Model TDS 420A) oscilloscope and a Velonex (Model 345) pulse generator. The sample was jacketed with rubber tubing to isolate it from the confining pressure medium. Piezoelectric (PZT) crystals mounted on steel endplates were used to generate P- and S-waves. The principal frequency was approximately 1 MHz for P-waves and 0.7 MHz for S-waves. A couplant was used to bond the endplates to the sample. The experimental configuration allowed simultaneous measurements of V_P and V_S at various confining pressures.

The value for V_P was picked from the first signal arrival, and V_S was picked on the first positive peak of the shear signal. The error in velocity measurement is estimated to be approximately 1% due to operator error in picking the first arrival. The system delay time was measured by taking head-to-head time at 2 MPa. The traveltime calibration was confirmed by measuring an aluminum cylinder at different pressures.

Confining pressure varied up to 40 MPa in increments of 5 MPa along loading and unloading cycles. At lower pressures (0–2.5 MPa), increments were of 0.5 MPa.

EXPERIMENTAL RESULTS

Porosity and grain density

Table 1 summarizes porosities and densities obtained in this study. Coal rock samples have low porosities ranging from 1.5 to 4.9%. In contrast, the powder sample has a porosity of 20%, which is very high compared to the rock samples.

Dry density ranges from 1.11 to 1.67 g/cm. Cannel coal has the lowest dry density whereas humic coals (bituminous, semianthracite, and anthracite samples) have dry densities that increase as rank increases. Density and porosity were calculated before pressurizing the samples.

Ultrasonic velocities

Laboratory data measured in different types/ranks of coal (Appendix A) show differences between velocities measured normal and parallel to lamination surfaces. They also show the effect of confining pressure in velocities. In addition, the data show a very important relationship between coal rank and elastic properties: The velocities increase as coal rank increases.

Velocities parallel to lamination surfaces are higher than velocities perpendicular to them and they increase with increasing confining pressure (Figures 1 and 2). We could not identify lamination surfaces on the anthracite sample, and the powder sample does not have any internal fabric. These two samples have the highest (anthracite) and the lowest (powder) velocities.

Pressure dependence of velocities on confining pressure is greater at pressures below 5 MPa. At higher pressures, velocities increase slightly. The highest variation with pressure is exhibited by the powder sample, with a velocity increase of approximately 35%.

In rock samples, velocities parallel to lamination surfaces increased between 4% and 20% as a function of confining pressure and velocities normal to lamination surfaces increased between 3% and 12%. Confining pressure was gradually increased from 0 to 40 MPa along loading and unloading cycles. During unloading cycles, velocities decreased following almost the same path of the velocities during the loading cycle. That was the case for most of the examples except the powder. Thus, rock samples showed a small hysteresis whereas the powder sample showed the largest hysteresis.

The humic coals used in this study are, in increasing order of rank, bituminous, semianthracite, and anthracite. From measured data, we

Table 1. Summary of the core plugs used in this study.

Sample Inventory					
Sample	Locality	Type/Rank	Orientation	Density (g/cc)	Porosity (%)
BKII	Breckenridge — KY	Cannel Coal	Parallel	1.14	1.8
BKpp	Breckenridge — KY	Cannel Coal	Perpendicular	1.11	2
HOpp	Hopkins — KY	Bituminous	Perpendicular	1.34	4.6
SCll	Spring Canyon — UT	Bituminous	Parallel	1.32	4.9
SCpp	Spring Canyon — UT	Bituminous	Perpendicular	1.3	4.1
BMII	Buck Mountain — CO	Semi-anthracite	Parallel	1.56	4.4
BMpp	Buck Mountain — CO	Semi-anthracite	Perpendicular	1.57	3.5
Bric	Briceño — Colombia	Anthracite	Undetermined	1.67	1.5
Gib	Gibson — IN	Bitum (powder)		1.2	20

observed that V_P and V_S increase as coal rank increases (Figure 3). Therefore, bituminous coal shows lower velocities than anthracite, which exhibits the highest velocities. On the other hand, cannel coal has similar velocities to bituminous coal.

Dynamic dry bulk modulus and dry shear modulus

Dry bulk moduli (Kdry) and dry shear moduli (Gdry) increase with confining pressure and coal rank, as shown in Figure 4 and Figure 5. These moduli are computed assuming constant density for the different confining pressures. In low-porosity rocks such as these coals, changes in porosity with confining pressure are related to the closing of microcracks. Consequently, those changes are small. The error in density is estimated to be less than 1%. The computed elastic moduli show small variations with respect to confining pressure compared to the effect of thermal maturity, even for pressures below 5 MPa. At higher pressures, changes in moduli are even smaller, reaching an asymptote. The larger variations in moduli are associat-

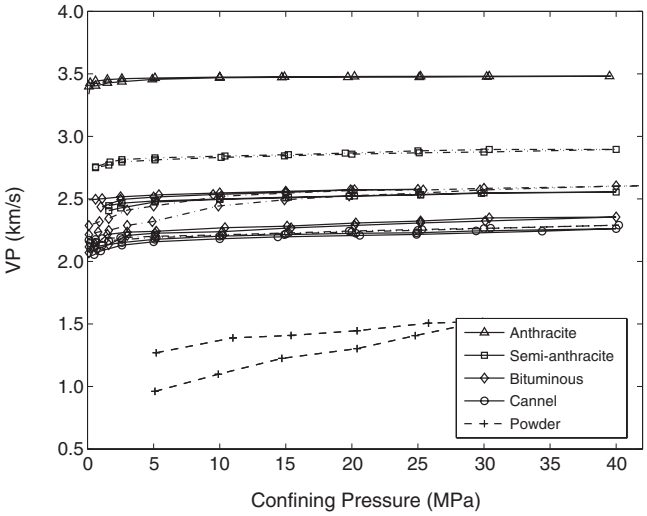

Figure 1. V_P as a function of confining pressure for core plugs parallel (solid lines) and perpendicular (dashed lines) to lamination surfaces. V_P increases as coal rank increases.

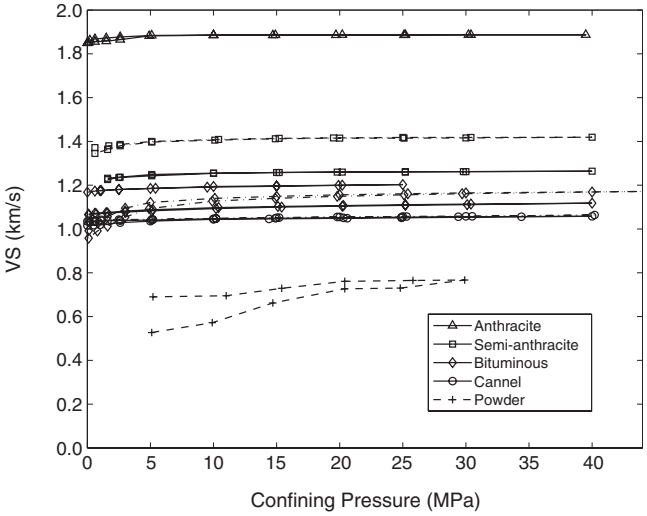

Figure 2. V_S as a function of confining pressure for core plugs parallel (solid lines) and perpendicular (dashed lines) to lamination surfaces.

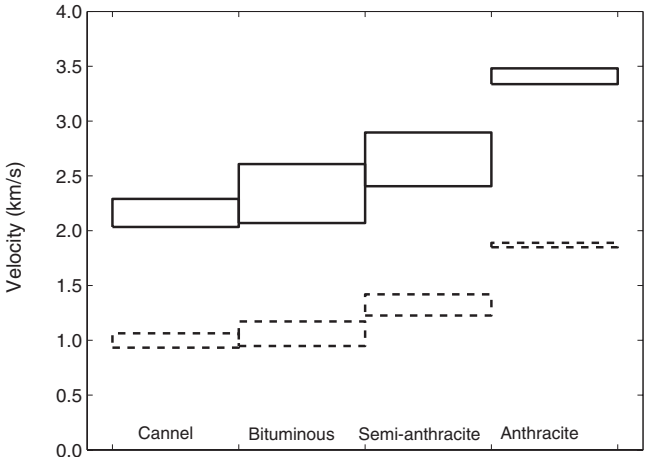

Figure 3. Range of velocity variation for different coal ranks. Solid boxes show the range of variation in V_P and dashed boxes show the range of variation in V_S. Note that velocities on humic coals increase as the coal rank increases.

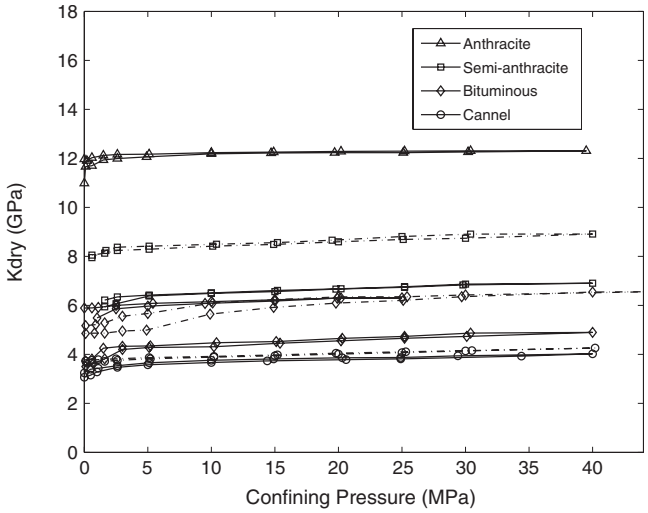

Figure 4. Calculated dry bulk modulus as a function of confining pressure. Note that dry bulk modulus increases as the coal rank increases.

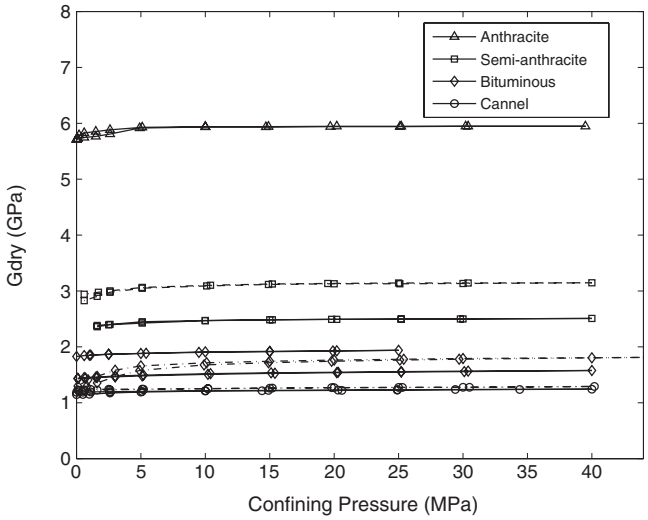

Figure 5. Calculated dry shear modulus as a function of confining pressure. Note that dry shear modulus increases as the coal rank increases.

ed with coal rank. Therefore, bituminous and cannel coals have lower moduli than semianthracite and anthracite, the latter of which has the highest rank and moduli.

V_P-V_S relationship

Figure 6 illustrates the V_P-V_S relationship for the data measured in this study acquired under dry conditions. The data show a linear trend that can be approximated by

$$V_S = 0.5774 * V_P 0.2088. \quad (1)$$

This regression follows a trend consistent for dry samples, from the high-porosity powder of bituminous coal to low-porosity anthracite. For zero shear velocity, the trend gives a P-wave velocity of 0.361 km/s.

In addition to the data obtained in this study, Figure 7 includes data reported by Greenhalgh and Emerson (1986), Yu et al. (1991), Castagna et al. (1993), Yu et al. (1993), and Yao and Han (2008). This compilation of coal-velocity data shows an empirical linear relationship that can be approximated by

$$V_S = 0.4811 * V_P + 0.00382. \quad (2)$$

Note that the measured data from this study are under dry conditions whereas the measured data from the aforementioned authors are under either dry or water-saturated conditions.

Figure 7 also shows the quadratic fit obtained by Castagna et al. (1993), which is given by

$$V_S = -0.232 * V_{P^2} + 1.5421 * V_P - 1.214. \quad (3)$$

Equations 1 and 2 are calibrated to high-porosity dry data from the powder sample whereas equation 3 tends to predict a trend for high-porosity water-saturated coal. However, equation 3 fails to predict the V_P-V_S ratio of semianthracite and anthracite.

The V_P-V_S ratio decreases as rank increases although this trend is erratic at low confining pressures (Figure 8). At confining pressures above 10 MPa, there is a consistent variation in the V_P-V_S ratio linked to coal rank. Anthracite has the lowest V_P-V_S ratio whereas bituminous coal has the highest V_P-V_S ratio.

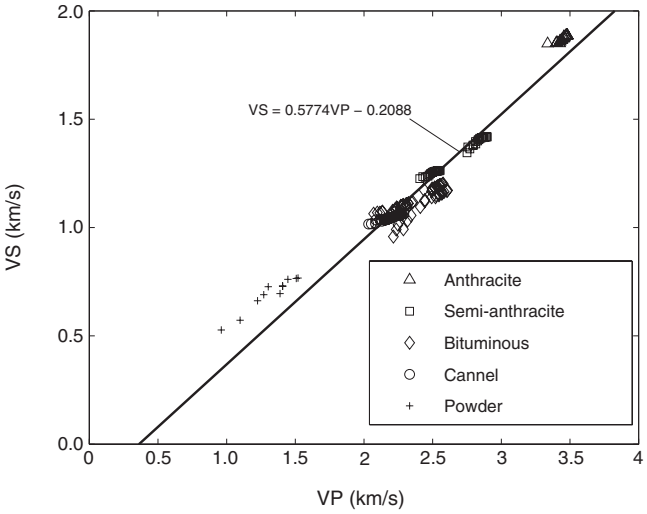

Figure 6. V_P versus V_S for dry samples measured in this study. The line shows the best linear fit for this data set.

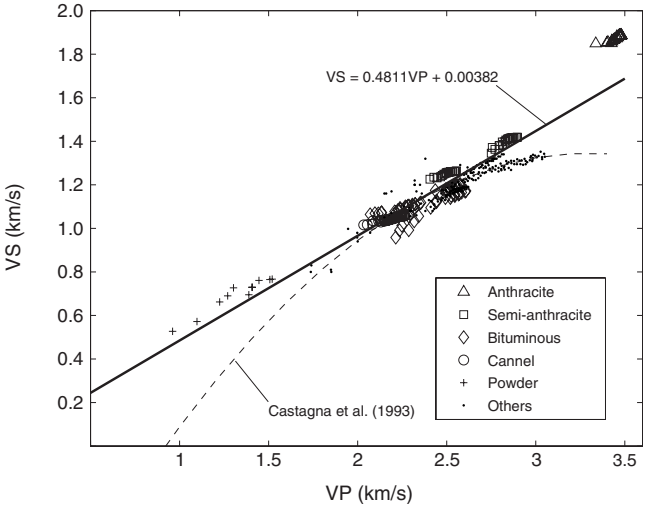

Figure 7. V_P versus V_S for different coals. The solid line corresponds to the best linear fit to all data, which includes dry and wet samples. For comparison purposes, the graph also shows the fit obtained for some bituminous coal samples by Castagna et al. (1993).

V_P and V_S anisotropy

Using velocity data from plugs parallel and perpendicular to lamination surfaces, we calculated P-wave and S-wave anisotropy using Thomsen's parameters. According to Thomsen (1986), P-wave anisotropy (ε) is given by

$$\varepsilon = \frac{V_P(90°) - V_P(0°)}{V_P(0°)}, \quad (4)$$

where V_P (90°) is V_P parallel to lamination surfaces and V_P (0°) is V_P perpendicular to lamination surfaces. Similarly, S-wave anisotropy (γ) can be obtained from

$$\gamma = \frac{V_S(90°) - V_S(0°)}{V_S(0°)}, \quad (5)$$

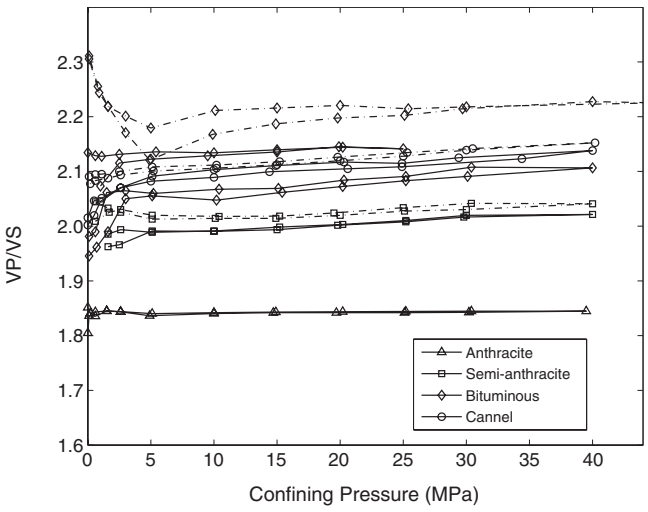

Figure 8. V_P/V_S ratio as a function of confining pressure for different types of coal. Note that the velocity ratio decreases as the coal rank increases.

where V_S (90°) is V_S parallel to lamination surfaces and V_S (0°) is V_S perpendicular to lamination surfaces.

Figure 9 shows P-wave and S-wave anisotropy as a function of confining pressure. As explained earlier, the dependence of velocities on confining pressure is greater at pressures below 5 MPa. However, at high confining pressures, bituminous coal and semianthracite show high anisotropy. Note that bituminous coal shows increasing anisotropy at low confining pressures.

DISCUSSION

In this study, pressure dependence of acoustic velocities is greater at pressures below 5 MPa. At higher confining pressures, velocities vary slightly. This finding is in agreement with the data reported by Yu et al. (1991) although in a later work Yu et al. (1993) report the dependence of velocities on confining pressure up to 10 MPa. The presence of pore space and microcracks tend to elastically soften the rock, producing a decrease in V_P and V_S (King, 1966). The gradual increase in velocities at low confining pressures is caused by the closure of microcracks. As the confining pressure increases, the rock frame gets stiffer, causing an increase in elastic properties.

The dependence of elastic properties on pressure shows an elastic and reversible behavior in the samples, except in the powder. In other words, by reducing the confining pressure (unloading cycle), the velocities decrease following almost the same path of the velocities during the loading cycle, causing little hysteresis. On the other hand, the powder exhibits larger hysteresis due to compaction.

We obtained a linear empirical V_P-V_S relationship for dry samples (equation 1), which covers a wide range of coal ranks, porosities, and effective confining pressures. Below 5 MPa, the V_P-V_S relationship shows variation as a function of pressure. Therefore, equation 1 should be used with caution at low confining pressures. In addition, we calculated another empirical V_P-V_S relationship (equation 2) that fits most of the data from this study (dry samples) and data from the aforementioned papers (wet and dry samples).

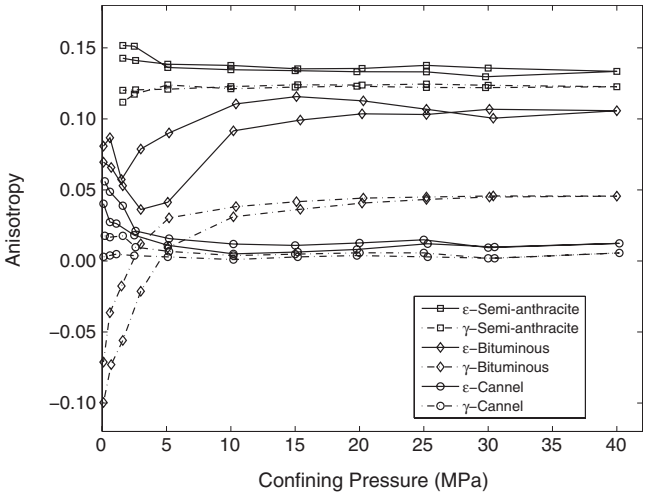

Figure 9. P-wave anisotropy (solid lines) and S-wave anisotropy (dashed lines) as a function of confining pressure for different coal ranks.

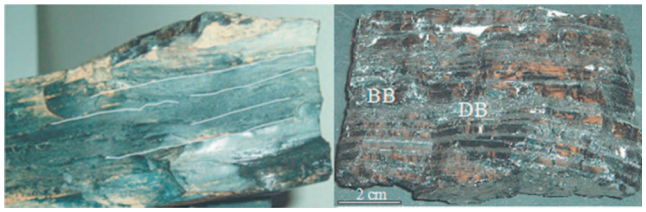

Figure 10. Sample of cannel coal (left) and bituminous coal (right) showing lamination. This bedding induces the intrinsic anisotropy observed in the samples. Bright bands (BB) and dull bands (DB).

Semianthracite and bituminous coal exhibit high P-wave and S-wave anisotropy that do not depend on cracks. When cracks are randomly oriented, the increase of velocity under increasing confining pressure should remain independent of direction. However, rocks with a nonrandom orientation of cracks will exhibit velocity anisotropy (Nur and Simmons, 1969), which should decrease as the cracks close under increasing confining pressure. The trends observed in Figure 1 and Figure 2 suggest that the cleats are closed when the confining pressure reaches a value of 5 MPa; however, the samples present significant anisotropy at pressures up to 40 MPa.

The simplest explanation for pressure dependence is the presence of compliant cracks or grain-to-grain contacts. Bedding anisotropy is enhanced by having horizontal cracks parallel to the bedding. Closing these cracks with pressure reduces the anisotropy. On the other hand, vertical open cracks tend to counteract the effect of bedding. In theory, enough vertical cracks can give negative ε and γ. Consequently, horizontal velocities can be smaller than vertical velocities. Sealing the vertical cleats via pressure causes the anisotropy to become more and more dominated by the fabric and can cause a shift from negative to positive ε and γ.

The anisotropy presented by the samples at high pressures seems to be related to fine-scale lamination (Figure 10) and the preferred orientation of the carbon-based minerals. As the coal rank increases, the carbon-based minerals get more oriented along lamination and the pore space decreases (Van Krevelen, 1993).

CONCLUSION

Coal thermal maturity has a significant influence on dynamic elastic properties of coal. Bituminous coal has lower velocities than semianthracite and anthracite; the latter has the highest rank and velocities. Dry bulk and dry shear moduli increase with increasing coal rank whereas the V_P-V_S ratio decreases with increasing coal rank.

Coal velocities also depend on confining pressure. The dependence of velocities on confining pressure is greater at lower pressures up to 5 MPa and is due to the presence of microcracks; above this pressure, changes in velocities are minimal.

The V_P-V_S relationship is empirical and is approximately linear over a wide range of velocities, coal ranks, and effective pressures. However, it should be used with caution at confining pressures lower than 5 MPa.

Semianthracite and bituminous coal exhibit high P-wave and S-wave anisotropy at high pressures that does not depend on the presence of cleats (cracks). The anisotropy at high pressures might be due to fine lamination and preferred orientation of the carbon minerals.

ACKNOWLEDGMENTS

This work was financially supported by the Stanford Rock Physics Laboratory and DOE (grant DE-FC26-01BC15354). Special thanks to Juan-Mauricio Florez, Kevin Wolf, Kyle Spikes, and Jorge Mejia. We also thank our Geophysics reviewers and the associated editor for their comments to improve the manuscript.

APPENDIX A

ULTRASONIC VELOCITY DATA AS A FUNCTION OF CONFINING PRESSURE

	Loading (UP)			Unloading (DOWN)		
Sample	Pc MPa	Vp km/s	Vs km/s	Pc MPa	Vp km/s	Vs km/s
Gib	0	0.948	0.511	0	0.984	0.545
Gib	2.1	0.951	0.512	2.6	0.989	0.545
Gib	5.1	0.961	0.525	5.2	1.088	0.55
Gib	9.9	1.098	0.572	11	1.389	0.695
Gib	14.7	1.26	0.662	15.4	1.408	0.729
Gib	20.4	1.327	0.727	20.4	1.452	0.747
Gib	24.8	1.407	0.73	25.8	1.477	0.765
Gib	27.9	1.502	0.767			
BKpp	0	2.034	0.933	0	2.086	0.952
BKpp	0.5	2.054	0.939	0.5	2.118	0.960
BKpp	1	2.084	0.948	1.1	2.127	0.963
BKpp	2.6	2.13	0.962	2.6	2.151	0.965
BKpp	5	2.157	0.970	5.1	2.177	0.971
BKpp	10	2.181	0.974	10	2.202	0.974
BKpp	14.4	2.196	0.979	14.9	2.214	0.980
BKpp	20.6	2.208	0.983	20.3	2.225	0.984
BKpp	24.9	2.216	0.984	24.9	2.229	0.985
BKpp	34.4	2.242	0.989	29.4	2.244	0.989
BKpp	40	2.262	0.993			
BKll	0.2	2.148	1.034	0.1	2.17	1.038
BKll	0.6	2.154	1.034	0.6	2.176	1.039
BKll	1.6	2.165	1.037	1.1	2.183	1.042
BKll	2.6	2.175	1.039	2.5	2.19	1.0429
BKll	5.2	2.191	1.043	5.1	2.201	1.044
BKll	10.2	2.207	1.048	10.2	2.213	1.048
BKll	15	2.22	1.051	15.2	2.228	1.052
BKll	20	2.236	1.055	19.8	2.243	1.055
BKll	25	2.249	1.057	25.3	2.256	1.057
BKll	30	2.263	1.058	30.5	2.266	1.058
BKll	40.2	2.29	1.064			
HOpp	1	2.436	1.175	0	2.493	1.168
HOpp	2.5	2.496	1.18	0.6	2.497	1.173
HOpp	5	2.515	1.185	1.1	2.502	1.176
HOpp	9.5	2.535	1.191	2.5	2.517	1.181
HOpp	15	2.552	1.195	5.4	2.533	1.186
HOpp	19.9	2.572	1.199	10	2.548	1.194
HOpp	25	2.576	1.203	15	2.561	1.197
HOpp				20.2	2.573	1.2
SCpp	0.1	2.07	1.064	0.1	2.116	1.068
SCpp	0.7	2.097	1.069	0.6	2.133	1.072
SCpp	1.6	2.135	1.073	1.5	2.216	1.075
SCpp	3	2.208	1.077	3	2.234	1.082
SCpp	5.1	2.226	1.083	5.2	2.241	1.088
SCpp	10.2	2.238	1.093	10.4	2.27	1.098

	Loading (UP)			Unloading (DOWN)		
Sample	Pc MPa	Vp km/s	Vs km/s	Pc MPa	Vp km/s	Vs km/s
SCpp	15.4	2.268	1.1	15.1	2.282	1.103
SCpp	20.2	2.288	1.104	20.3	2.307	1.107
SCpp	25.2	2.308	1.108	25.2	2.323	1.111
SCpp	30.1	2.323	1.111	30.4	2.348	1.114
SCpp	40	2.355	1.118			
SCll	0.1	2.214	0.958	0.1	2.287	1.033
SCll	0.8	2.235	0.991	0.9	2.318	1.036
SCll	1.6	2.248	1.013	1.6	2.343	1.056
SCll	3	2.288	1.054	3	2.41	1.095
SCll	4.9	2.318	1.093	5	2.443	1.121
SCll	9.9	2.443	1.127	10.1	2.521	1.14
SCll	14.9	2.493	1.14	15	2.546	1.149
SCll	19.8	2.525	1.149	20	2.567	1.156
SCll	25.1	2.546	1.156	25.4	2.571	1.161
SCll	29.7	2.571	1.161	30	2.584	1.165
SCll	40	2.604	1.169			
SCll	45	2.608	1.172			
BMpp	1.6	2.406	1.226	1.6	2.446	1.232
BMpp	2.5	2.428	1.235	2.6	2.468	1.237
BMpp	5.1	2.475	1.243	5.1	2.49	1.249
BMpp	10	2.496	1.254	10	2.499	1.255
BMpp	15	2.51	1.258	15.2	2.505	1.258
BMpp	19.8	2.522	1.26	20.2	2.52	1.26
BMpp	25.2	2.532	1.261	25.2	2.535	1.261
BMpp	29.8	2.545	1.262	30	2.549	1.262
BMpp	40	2.555	1.264			
BMll	0.6	2.75	1.345	0.6	2.756	1.372
BMll	1.6	2.771	1.363	1.7	2.795	1.38
BMll	2.6	2.795	1.38	2.6	2.814	1.386
BMll	5.1	2.812	1.397	5.1	2.828	1.397
BMll	10.1	2.832	1.406	10.4	2.843	1.409
BMll	14.9	2.844	1.412	15.2	2.854	1.414
BMll	20	2.858	1.415	19.5	2.866	1.416
BMll	25.1	2.869	1.415	25	2.884	1.418
BMll	30	2.875	1.416	30.4	2.895	1.418
BMll	40	2.896	1.419			
Bric	0	3.337	1.849	0	3.425	1.85
Bric	0.1	3.399	1.851	0.2	3.428	1.862
Bric	0.6	3.405	1.855	0.6	3.443	1.868
Bric	1.5	3.428	1.858	1.5	3.454	1.872
Bric	2.6	3.438	1.865	2.6	3.461	1.877
Bric	4.9	3.456	1.882	5.1	3.467	1.884
Bric	10	3.469	1.885	10	3.474	1.886
Bric	14.7	3.472	1.885	14.9	3.476	1.886
Bric	19.7	3.474	1.886	20.2	3.479	1.887
Bric	25.1	3.474	1.886	25.2	3.48	1.887
Bric	30.2	3.477	1.887	30.4	3.481	1.887
Bric	39.5	3.481	1.887			

REFERENCES

Birch, F., 1960, The velocity of compressional waves in rocks to 10 kilobars, Part 1: Journal of Geophysical Research, **65**, no. 4, 1083–1102, doi: 1029/JZ065i004p01083.

Castagna, J. P., M. L. Batzle, and T. K. Kan, 1993, Rock physics: The link between rock properties and AVO response, in J. P. Castagna, and M. Backus, eds., Offset-dependent reflectivity — Theory and practice of AVO analysis: SEG, 135–171.

Greenhalgh, S. A., and D. W. Emerson, 1986, Elastic properties of coal measure rock from the Sydney Basin, New South Wales: Exploration Geophysics, **17**, no. 3, 157–163, , doi: 10.1071/EG986157.

King, M. S., 1966, Wave velocities in rocks as a function of overburden pressure and pore fluid saturants: Geophysics, **31**, 56–73, doi: 10.1190/1.1439763.

Nur, A., and G. Simmons, 1969, Stress-induced velocity anisotropy in rocks: An experimental study: Journal of Geophysical Research, **74**, no. 27, 6667–6674, doi: 10.1029/JB074i027p06667.

Thomsen, L., 1986, Weak elastic anisotropy: Geophysics, **51**, 1954–1966, doi: 10.1190/1.1442051.

Van Krevelen, D. W., 1993, Coal: Typology physics chemistry constitution, Third edition: Elsevier.

Yao, Q., and D. Han, 2008, Acoustic properties of coal from lab measurement: 80th Annual International Meeting, SEG, Expanded Abstracts, 27, 1815–1819.

Yu, G., K. Vozoff, and D. W. Durney, 1991, Effects of confining pressure and water saturation on ultrasonic compressional wave velocities in coals: International Journal of Rock Mechanics and Mining Sciences, **28**, no. 6, 515–522, doi: 10.1016/0148-9062(91)91127-D.

———, 1993, The influence of confining pressure and water saturation on dynamic elastic properties of some Permian coals: Geophysics, **58**, 30–38, doi: 10.1190/1.1443349.